Journal of Non-Crystalline Solids 664 (2025) 123587

Contents lists available at ScienceDirect

Journal of Non-Crystalline Solids

journal homepage: www.elsevier.com/locate/jnoncrysol

Preparation and characterization of luminiscent layers of TEOS micro/nanofibers with Sm_2O_3 for potential usage in photodynamic therapy

Aiman Albekova *, Martin Havlík Míka, Kristýna Jílková, Richard Bursa, Dominika Fink

University of Chemistry and Technology, Department of Glass and Ceramics, Technická 5, 166 28 Prague, Czech Republic

ARTICLE INFO

Keywords:
Glass
Micro/nanofibers layers
Electrospinning
Luminescence

ABSTRACT

One of the most important and latest directions of scientific and technological progress is the creation and production of new materials. The main trend remains in the development of materials with improved properties through the application of nanotechnology. The last 20 years of scientific research have demonstrated the significant role of nanotechnology in various fields of science and technology, including biology and medicine. This paper is devoted to the production and characterization of micro/nanofiber layers containing microparticles and nanoparticles of luminescent glasses, suitable for the application in photodynamic therapy.

1. Introduction

Nanotechnology is currently experiencing dynamic growth. This rapidly evolving field focuses on the study of materials at the nanoscale, typically measured in nanometers [1]. Nanotechnology has significant implications across multiple scientific disciplines, including physics, chemistry, and molecular biology. The applications of nanomaterials are extensive and diverse, ranging from electronics to the chemical industry. In medicine, the ability of nanoparticles to deeply penetrate tissues, cells, and nuclei can be particularly beneficial [2–5]. The advancements in molecular diagnostics and the identification of patient-specific biomarkers pave the way for improved therapies and targeted drug delivery. However, the increasing use of nanotechnology necessitates the study of nanoparticle safety and the assessment of their toxic effects on the environment and human health [6–8].

Nanofibers are structures with diameters on the nanometer scale, typically between 100 and 800 nanometers [9,10]. These fibers can be derived from various polymers, leading to different physical properties and applications. Natural polymers used to create nanofibers include collagen, cellulose, silk fibroin, keratin, gelatin, and polysaccharides such as chitosan and alginate. Synthetic polymers include polylactic acid (PLA), polycaprolactone (PCL), polyurethane (PU), poly(lactic-co-glycolic acid) (PLGA), poly(3-hydroxybutyrate-co-3-hydroxyvalerate) (PHBV), and poly (ethylene-vinyl acetate) (PEVA). The diameter of nanofibers depends on the type of polymer used and the production method [11–16].

Polymeric nanofibers are unique due to their high surface area to volume ratio, significant porosity, notable mechanical strength, and flexibility in functionalization compared to their microfiber counterparts [17,18]. Nanofibers prepared by electrospinning have shown to mimic and behave similarly to the extracellular matrix. As a culture medium, they stimulate cell growth and allow the formation of organized cellular structures [19–21]. The small diameter of electrospun nanofibers, which closely matches that of the extracellular matrix, and their high surface area to volume ratio make them ideal for cell attachment, proliferation, and differentiation. These unique properties of electrospun nanofibers make them suitable for various medical applications [22–27]. Photodynamic therapy (PDT) is a clinically utilized treatment approach that combines light, oxygen, and a photosensitizing agent to selectively destroy cancer cells. The process involves the activation of a photosensitizer by a specific wavelength of light, leading to the generation of reactive oxygen species (ROS) that induce cellular damage and apoptosis. PDT has shown significant promise in treating various types of cancers, skin disorders, and infections.

Recent research has explored the use of micro- and nanofibers in PDT to improve the delivery and targeting of photosensitizers. These fibers, due to their tunable properties, offer excellent drug-loading capabilities and facilitate better control over the release of therapeutic agents. Additionally, their small size allows them to penetrate deeper into tissues, enhancing the treatment's effectiveness and minimizing collateral damage to surrounding healthy cells. Nanofiber-based PDT systems, often created using biocompatible and biodegradable materials, have gained attention for their ability to enhance the localization and accumulation of photosensitizers at the tumor site. These fibers can be loaded with photosensitizers and administered directly to the target area,

* Corresponding author.
E-mail address: albekova@vscht.cz (A. Albekova).

https://doi.org/10.1016/j.jnoncrysol.2025.123587
Received 11 February 2025; Received in revised form 28 April 2025; Accepted 28 April 2025
Available online 17 May 2025

Table 1
The atomic composition of the glass batches [%].

Glass composition without oxygen [at. %]	Na	Zn	Al	Si	Ge	Eu	Sm	Ca	P	Mg	Sum
G01	36.68	00.00	00.00	35.14	00.00	00.00	0.54	10.68	3.63	13.33	100.00
G02	36.68	24.16	00.00	35.00	00.00	00.00	0.54	00.00	3.62	00.00	100.00
G03	29.83	22.53	00.00	34.59	00.00	00.00	0.54	3.50	9.02	00.00	100.00
G04	37.01	23.00	00.00	35.32	00.00	00.00	0.55	1.25	1.83	1.04	100.00
G05	23.53	9.80	1.96	62.75	00.00	1.96	00.00	00.00	00.00	00.00	100.00
G06	23.53	9.80	1.96	52.94	9.80	1.96	00.00	00.00	00.00	00.00	100.00

Table 2
Composition of the glass batches [g].

Glass composition [g]	G01	G02	G03	G04	G05	G06
Na_2CO_3	00.00	00.00	16.83	17.26	125.54	10.78
Na_2SO_4	24.00	20.45	00.00	00.00	00.00	00.00
ZnO	00.00	35.38	33.38	33.38	75.35	6.47
$Al(OH)_3$	00.00	00.00	00.00	00.00	14.67	1.26
SiO_2	44.58	37.84	37.84	37.84	300.00	25.76
GeO_2	00.00	00.00	00.00	00.00	00.00	8.29
Eu_2O_3	00.00	00.00	00.00	00.00	32.49	2.79
Sm_2O_3	2.00	1.70	1.70	1.70	00.00	00.00
$CaCO_3$	12.64	00.00	3.57	2.23	00.00	00.00
$NaH_2PO_4{\cdot}2H_2O$	5.44	4.63	23.31	23.31	00.00	00.00
MgO	11.34	00.00	00.00	0.76	00.00	00.00
Sum	100.00	100.00	116.63	116.48	548.06	55.35

Table 3
Used chemicals for glass batches.

Raw materials	Chemical formula	Manufacturer	M [g/mol]
Sodium sulfate	Na_2SO_4	Penta	142.04
Calcium carbonate	$CaCO_3$	Lachema	100.09
Magnesium oxide	MgO	Lachema	40.32
Silica gel	SiO_2	Acros organics	60.08
Zinc oxide	ZnO	Lachema	81.38
Sodium dihydrogen phosphate	$NaH_2PO_4{\cdot}2H_2O$	Penta	156.01
Samarium (III) oxide	Sm_2O_3	Puralab	348.72
Europium (III) oxide	Eu_2O_3	Puralab	351.92
Germanium dioxide	GeO_2	Puralab	104.61
Aluminum oxide	$Al(OH)_3$	Lachema	78.00
Sodium carbonate	Na_2CO_3	Lachema	105.99

ensuring precise treatment with reduced systemic side effects [28–31].

In addition to the above developments, recent research has highlighted the potential of luminescent materials for enhancing photodynamic therapy (PDT) [32]. Specifically, incorporating rare-earth elements such as samarium oxide (Sm_2O_3) into glass-based nanofibers has proven effective in producing stable orange-red emissions, which are well-suited for biomedical imaging and therapeutic applications. This emission range is particularly beneficial for PDT due to its deep tissue penetration and efficient activation of photosensitizers [33].

Silica-based glasses derived from tetraethyl orthosilicate (TEOS) serve as excellent hosts for rare-earth dopants, offering optical transparency, biocompatibility, and structural stability. When fabricated via electrospinning, TEOS-based sol-gel systems yield uniform nanofiber layers with high surface area and tunable porosity. These characteristics make them ideal platforms for incorporating luminescent agents while preserving fiber morphology and luminescent efficiency even after thermal treatment [34–35].

Studies have shown that Sm^{3+}-doped silica nanofibers retain their luminescent properties post-calcination, and their emission intensity and stability can be tuned by adjusting dopant distribution and concentration [34]. Such fibers can function as both drug delivery vehicles and internal light sources, supporting synergistic effects in PDT. Moreover, their chemical and mechanical resilience ensures functionality under physiological conditions [35].

Future directions in this area include the development of multifunctional nanofiber systems capable of combining therapy, imaging, and real-time diagnostic feedback. Enhancing biocompatibility, optimizing dopant levels, and improving uniformity of luminescent particle dispersion remain key areas of focus for bringing these materials closer to clinical use [36–37].

In this study, were prepared electrospun micro/nanofibers composed of TEOS, PVP and powder of synthesized six phosphor glasses with varying chemical compositions, focusing on samarium oxide as a primary dopant. The goal was to evaluate the prepared fibers their luminescent properties and determine which composition would be most suitable for use in PDT. By exploring the role of samarium oxide in optimizing luminescence, we aim to push forward the development of materials that enhance light-based therapies in the medical field.

2. Experimental

2.1. Preparation of glasses

The preparation of glasses by melting involved several steps. First, the relevant raw materials were weighed out (according to Table 1–3 and their mixture was homogenized for 10 minutes in a porcelain mortar to obtain homogenous glass batch. The raw materials used for the preparation of glasses were sodium carbonate, magnesium oxide, calcium carbonate, silica gel, zinc oxide, sodium dihydrogen phosphate, samarium oxide. The glass batch was gradually loaded into a PtRh crucible. The crucible, covered with a lid, was placed in an electric furnace with Superkanthal heating elements, where the glass batch was melted at a temperature of 1480 °C. Melting proceeded for one hour initially. After one hour, the melt was regularly stirred by circular movement of the crucible. The melt was stirred every 15 minutes, a total of 5 times. After melting was completed, the melt was poured into a stainless-steel mould, where it solidified into the shape of an ingot. Subsequently, the ingot was placed in a tempering furnace. To remove internal stress, the ingot was tempered at a temperature of 520 °C for 1 hour. The ingot was then cooled to room temperature over the course of the next day.

2.1.1. Grinding of glass

For the production of micro/nanofibers from carrier polymers with glass particles, it was necessary to grind the glass into the smallest possible particles. A zirconia (ZrO_2) grinding jar with zirconia grinding balls of 5 mm in diameter from LOID was used for grinding the selected glass. An extremely high-energy ball mill, Retsch E-MAX, capable of grinding particles down to the nanometer range, was employed for this purpose. The grinding was conducted for 10 minutes at a speed of 800 revolutions per minute. The weight ratio of glass to grinding balls in the jar was 1:15. Before grinding, the glass was crushed into smaller shards using a hammer in an iron mortar to facilitate the grinding of most of the sample. After grinding, the particle size distributions of the samples were evaluated using a laser confocal microscope Olympus OLS5000. A very small amount of powdered sample was placed into a

Table 4
Formulations of solutions for preparing TEOS solution.

Type of solution	$m_{HCl\ (36\ \%)}$ [g]	m_{H2O}[g]	m_{EtOH}[g]	m_{TEOS}[g]
Titration solution	0.08	4.92	8.71	00.00
TEOS solution	00.00	00.00	8.71	50.00

Table 5
Used chemicals for micro/nanofibers.

Raw materials	Chemical formula	Manufacturer	M [g/mol]
Tetraethyl orthosilicate	$C_8H_{20}O_4Si$	Sigma Aldrich	208.33
Polyvinylpyrrolidone	$(C_6H_9NO)_n$	Sigma Aldrich	1300,000.00

Table 6
Electrospinning device parameters.

Needle and collector distance	15 cm
Voltage	20 kV
Extrusion speed	1 ml/h
Volume of solution per sample	2 ml
Inner diameter of the needle	1.067 mm

Table 7
Elemental composition of selected points obtained by EDS analysis of the G01 sample.

Element	Spectrum 5 [wt. %]	Spectrum 6 [wt. %]	Spectrum 7 [wt. %]	Spectrum 8 [wt. %]	Spectrum 9 [wt. %]
O	34.6	50.7	53.2	54.7	54.4
Si	36.5	34.5	39.6	42.3	45.5
Na	25.3	2.4	3.2	3.0	3.1
Sm	–	2.3	–	–	–
Ca	3.6	5.1	2.0	–	–
Al	–	–	–	–	–
Mg	–	5.0	2.0	–	–

microcentrifuge tube and filled with isopropyl alcohol to a final volume of 1.5 ml. The microcentrifuge tube was placed in an ultrasonic bath for 3 minutes to disperse the sample. Subsequently, one drop of the sample was placed on a microscope slide and allowed to air-dry to evaporate the solvent. The sample was scanned using a microscope, and data was generated using the Particle Analysis tool, which was then converted into individual particle sizes using software. The analysis results are based on measurements of at least 5000 particles.

2.1.2. Preparation of the solution for fiber spinning

The spinning solution consisted of two components—TEOS (tetraethyl orthosilicate) and PVP (polyvinylpyrrolidone)—to which ground glass particles were added. The TEOS and PVP solutions were prepared separately and then mixed together in the appropriate ratio to achieve the desired viscosity, ranging from 0.120 to 0.200 Pa·s.

2.1.3. Preparation of TEOS solution

To prepare the TEOS solution for fiber spinning, an acidified titration solution of ethanol (denatured with methanol) and distilled water was first prepared. Separately, TEOS was mixed with ethanol in another container and then homogenized by stirring. This homogenized TEOS-ethanol mixture was then slowly titrated with the acidified ethanol-water solution while stirring gently. The formulations for these solutions are provided in Table 4. The solution was then stored in the refrigerator, where it remains usable for electrospinning even after several months.

Table 5
Table 6
Table 7
Table 8
Table 9
Table 10
Table 11
Table 12

Table 9
Elemental composition of selected points obtained by EDS analysis of the G03 sample.

Element	Spectrum 1 [wt. %]	Spectrum 2 [wt. %]	Spectrum 3 [wt. %]
O	48.4	50.2	52.9
Si	42.1	33.1	34.6
Zn	6.6	11.4	8.3
Sm	–	1.3	0.9
Na	2.9	2.4	2.1
Ca	–	1.6	1.2

Table 10
Elemental composition of selected points obtained by EDS analysis of the G04 sample.

Element	Spectrum 2 [wt. %]	Spectrum 4 [wt. %]	Spectrum 7 [wt. %]	Spectrum 8 [wt. %]	Spectrum 9 [wt. %]
O	40.7	45.2	47.4	48.8	49.2
Si	51.3	31.8	45.6	42.2	37.4
Zn	4.0	16.7	3.8	5.7	6.0
Sm	–	1.2	–	–	1.7
Na	3.3	5.1	3.2	2.4	5.7
Al	–	–	–	–	–
Ca	0.7	–	–	1.0	–

Table 11
Elemental composition of selected points obtained by EDS analysis of the G05 sample.

Element	Spectrum 1 [wt. %]	Spectrum 2 [wt. %]	Spectrum 3 [wt. %]	Spectrum 4 [wt. %]	Spectrum 5 [wt. %]
O	21.8	38.6	44.5	31.0	45.6
Si	32.1	42.6	48.1	28.1	45.0
Zn	4.3	7.2	2.9	2.3	3.1
Eu	2.9	7.0	1.9	–	2.6
Na	38.1	3.5	2.7	1.7	3.7
Al	0.9	1.2	–	–	–
C	–	–	–	3.4	–
Cl	–	–	–	3.6	–
Au	–	–	–	27.4	–

Table 8
Elemental composition of selected points obtained by EDS analysis of the G02 sample.

Element	Spectrum 1 [wt. %]	Spectrum 2 [wt. %]	Spectrum 3 [wt. %]	Spectrum 4 [wt. %]	Spectrum 5 [wt. %]	Spectrum 6 [wt. %]	Spectrum 7 [wt. %]
O	45.6	47.9	34.7	41.8	44.2	47.3	46.2
Si	37.0	46.2	34.2	29.7	33.6	47.4	39.8
Zn	12.3	4.3	25.7	23.5	12.1	4.0	10.7
Sm	1.9	–	2.4	1.5	2.0	–	–
Na	3.2	1.6	3.0	3.5	1.9	1.3	3.3
C	–	–	–	–	6.2	–	–

Table 12
Elemental composition of selected points obtained by EDS analysis of the G06 sample.

Element	Spectrum 1 [wt. %]	Spectrum 2 [wt. %]	Spectrum 3 [wt. %]	Spectrum 4 [wt. %]
O	47.0	33.0	46.9	48.6
Si	32.3	34.5	48.3	46.9
Zn	10.6	–	1.9	1.8
Eu	5.5	6.5	–	–
Na	3.6	12.2	0.6	0.6
Al	1.0	–	–	–
Ge	–	13.8	2.4	2.2

EDS was used to verify the composition of the fibers and glass particles for each sample. For samples G01 to G04, samarium atoms were detected inside the particles, while for samples G05 and G06, europium atoms were detected. The spectra of the fibers without particles contained 40–50 % silicon and 40–50 % oxygen in most measurements.

Fig. 1. Electrospinning device EF050 Needle Starter Kit.

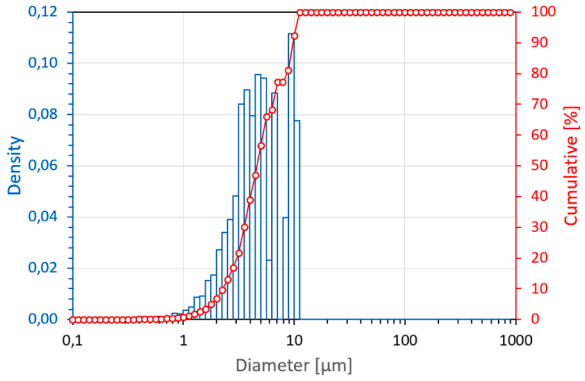

Fig. 2. Particle size distribution of glass G01.

2.1.4. Preparation of PVP solution

A solution of polyvinylpyrrolidone (PVP) was prepared in a weight ratio of 1:6 with ethanol. The PVP was added to the ethanol and left to dissolve under stirring until a clear solution was obtained.

2.1.5. Preparation of the solution for electrospinning

The TEOS and PVP solutions were mixed in a weight ratio of 2:2,5:1 (TEOS:PVP:glass particles). First, the PVP and TEOS solutions were combined and allowed to homogenize under stirring for 10 minutes. In the second step, the ground glass particles were added, and the solution was stirred for an additional 10 minutes. The third step involved placing the solution in an ultrasonic bath for 3 minutes to increase its viscosity. After removing the solution from the ultrasonic bath, it was stirred again for 10 minutes.

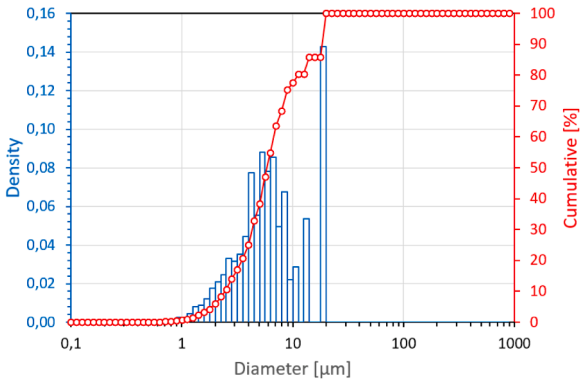

Fig. 3. Particle size distribution of glass G02.

2.2. Electrospinning

The prepared solution for electrospinning was drawn into a 10 ml syringe, which was then placed into a syringe pump (Fig. 1, left). An aluminum foil was placed in front of the metal collector (Fig. 1, right), and a glass fiber mesh was secured onto the foil using rubber bands. The micro/nanofibers were collected on this mesh. A stainless-steel needle, gauge 17 with a blunt end, was positioned at the center of the setup. A high-voltage power supply was connected to this needle, with the other contact attached to the metal collector of the device (Fig. 1, right). The solution was pumped from the syringe through a tube into the needle, where the polymer solution received an electrical charge. The polymer drop at the needle tip was then deformed by electrical forces into a Taylor cone, from which micro/nanofibers were formed as they flew from the needle tip to the metal collector (Fig. 1). The resulting micro/nanofiber layer was left to air dry overnight to remove any remaining solvent. The dried layer was then calcined in a furnace at 650 °C for 1 hour, with a temperature ramp of 1 °C per minute, to calcine the TEOS and burn out the PVP, resulting in a purely inorganic product.

2.2.1. Parameters of electrospinning device

2.3. Characterization of the prepared micro/nanofiber layers

2.3.1. Laser confocal microscope

To capture images using the Olympus LEXT OLS5000 laser confocal microscope, a small section of the prepared micro/nanofiber layer was cut and attached to a glass slide for imaging. Various magnification levels and 3D scans were obtained, as the fibers are layered. Images of the samples were collected both before and after firing, but the paper only includes the results obtained after firing.

2.3.2. Scanning electron microscopy (SEM) and energy dispersive spectroscopy (EDS)

For imaging using the TESCAN MIRA SEM, a small piece of the prepared micro/nanofiber layer was detached and secured to a carbon tape on a stub, followed by gold coating. Various magnifications were employed to capture images that highlighted different fiber details in both secondary electron (SE) mode and backscattered electron (BSE) mode. The fiber and glass particle compositions in the samples were verified through EDS point analysis, with measurement errors ranging from 0.1 to 0.7 weight percent for each element. Images were obtained for the samples both prior to and after firing.

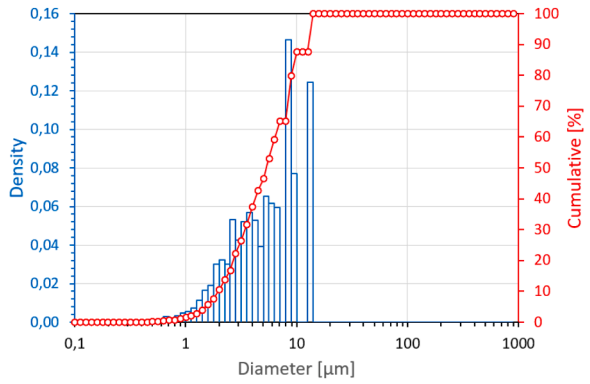

Fig. 4. Particle size distribution of glass G03.

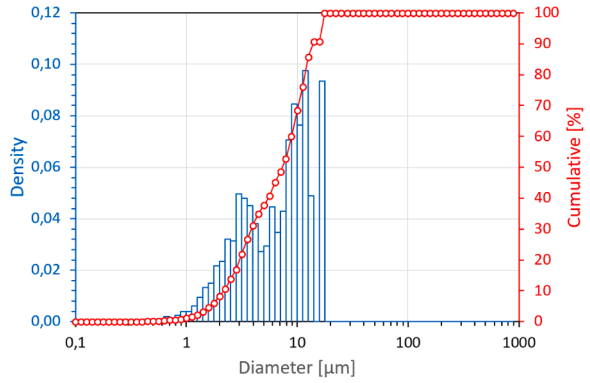

Fig. 5. Particle size distribution of glass G04.

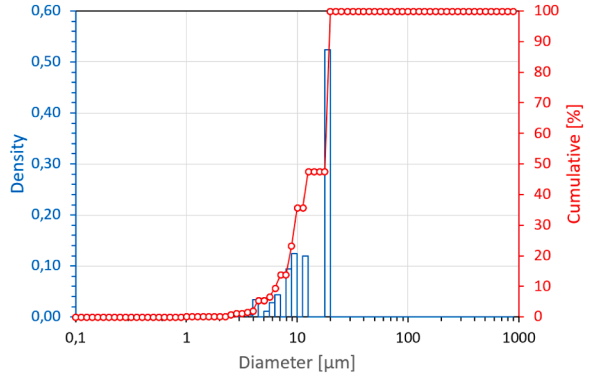

Fig. 6. Particle size distribution of glass G05.

2.3.3. *Transmittance spectra*

The transmittance spectra of all glass samples were recorded in the visible (VIS) region using a UV–VIS-NIR spectrophotometer (UV-3600, Shimadzu). Data were collected with a 1 nm step size.

3. Results and discussion

3.1. *Glass grinding*

Figs. 2–7 illustrate the results of the glass grinding process, presented as particle size distribution graphs. Grinding with the high-energy E-MAX mill resulted in particles ranging from a few to several tens of micrometers. For glasses G01 to G04, 70 % of the particles are smaller than 10 micrometers. In contrast, for glass G05, only 25 % of the particles are smaller than 10 micrometers, while all particles in glass G06 fall within the 10–25 micrometer range. These variations are likely due to the different compositions of the glasses, particularly the phosphorus content in glasses G01 to G04. In comparison, glasses G05 and G06 are silica glasses without phosphorus, as the grinding conditions were identical for each sample.

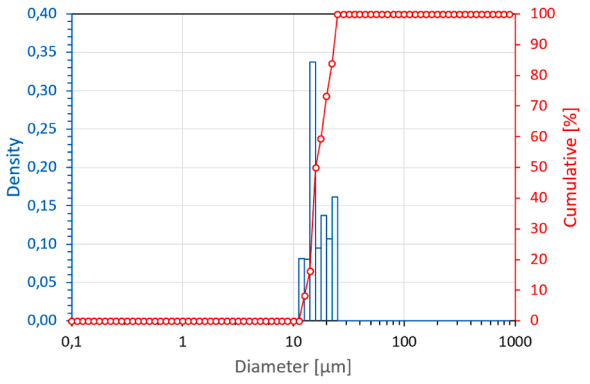

Fig. 7. Particle size distribution of glass G06.

3.2. *Characterization of the prepared micro/nanofiber layers*

3.2.1. *Images of micro/nanofiber layers*

To characterize the micro/nanofibers and determine the morphology of their surface, images were taken using a laser confocal microscope and a scanning electron microscope. Fig. 8a shows the layer just moments after being produced by electrospinning. This layer is highly flexible, bendable, and relatively strong, but it is water-soluble due to the presence of organic polyvinylpyrrolidone in the micro/nanofibers. After high-temperature pyrolysis, which is necessary to calcinate the organic components and sinter the TEOS, the layer becomes significantly more brittle and less flexible. However, it then consists solely of inorganic components – silica and glass particles – granting it high thermal and chemical resistance.

3.2.2. *Laser confocal microscope*

The fired layers were subsequently analyzed using optical and electron microscopy to determine the thickness (average circular cross-section) of the micro/nanofibers, as well as their structure, defects, surface morphology, and to verify the composition of the glass particles and fibers after firing in the furnace. Figs. 9–14 contain images taken with the laser confocal microscope in the visible spectrum. Figs. 15–20 show images obtained via scanning electron microscopy and EDS analysis. In images with lower magnification, a dense network of micro/nanofibers can be observed, with scattered glass particles visible at higher magnifications. The glass particles are either adhered to the fibers or directly encapsulated by the polymer fibers. These particles tend to cluster into larger aggregates. Certain defects in the fibers, such as broken fibers and granules, contribute to the layer's brittleness aside from the burnout of polyvinylpyrrolidone. Fig. 19b provides a detailed view of the surface of submicron fibers, revealing a porous surface, with fiber diameters ranging from hundreds of nanometers to several micrometers (e.g., Fig. 20b). This variability is mainly due to the inability to maintain constant laboratory conditions – particularly temperature, humidity, and the degree of crosslinking in the TEOS solution.

The images also show considerable free space, which could potentially be used to add more particles by adjusting the initial solutions for electrospinning, spraying particles directly, or pressing multiple layers together to densify the particles and fibers. This would be desirable to

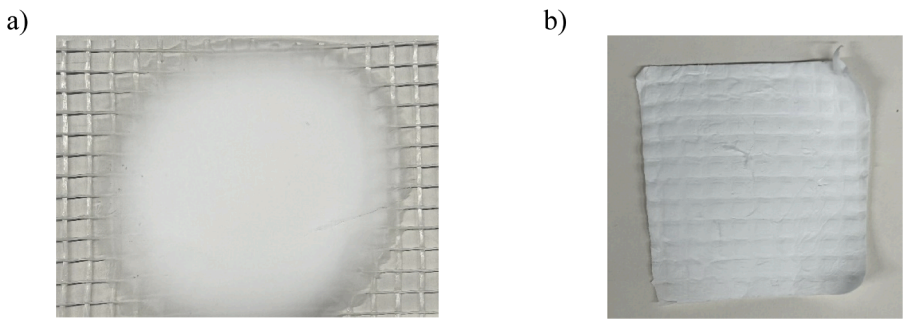

Fig. 8. a). Layer of micro/nanofibers prepared by electrospinning a solution of PVP, TEOS, and glass particles of G06, b) Sample of the micro/nanofiber layer after firing in a furnace containing TEOS and glass particles of G06.

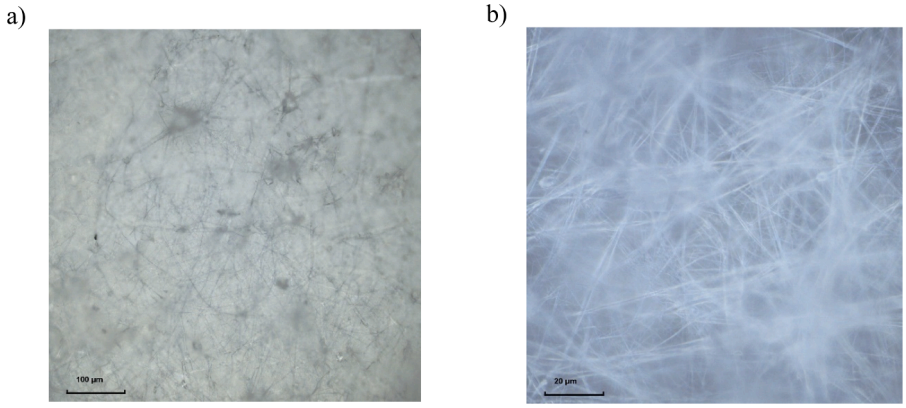

Fig. 9. Image of the G01 sample after firing in a furnace taken with a confocal microscope, magnification a) 20x, b) 100x.

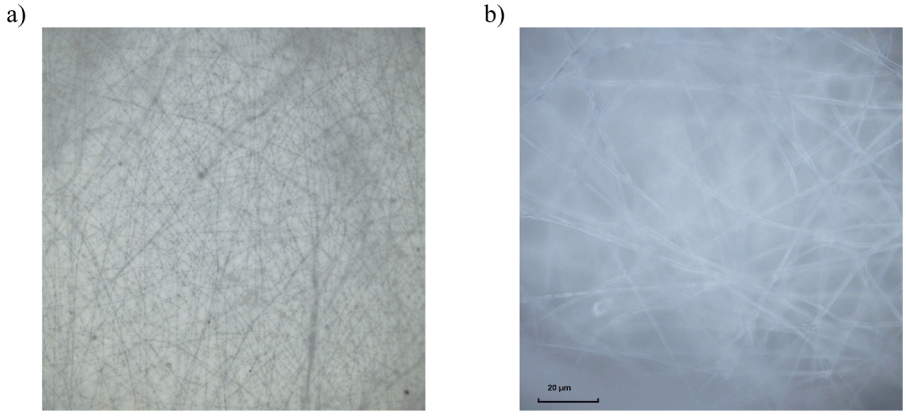

Fig. 10. Image of the G02 sample after firing in a furnace taken with a confocal microscope, magnification a) 20x, b)100x.

increase the luminescence intensity for measuring singlet oxygen generation in solutions with photosensitive substances in subsequent academic studies.

3.2.3. Scanning electron microscopy with EDS

3.2.4. Transmittance spectra

The transmittance spectra are shown in Fig. 21. In samples containing samarium atoms (G01-G04), absorption bands can be observed around wavelengths of 472 nm and 401 nm. In samples containing europium atoms (G05 and G06), the absorption bands are shifted; the first absorption band appears at a wavelength 465 nm, and second at 393 nm. These absorption bands perfectly match the transmittance and excitation spectra measurements performed in previous studies, where the compositions of glasses G01 – G06 were first used and measured on polished glass blocks, confirming the ability of glass particles inside the nanofiber layer to absorb radiation [38-40]. The transmittance values on the "y" axis vary, ranging from 0 to 6 %. These differences are due to the varying thicknesses of the analyzed layers as well as the different fiber

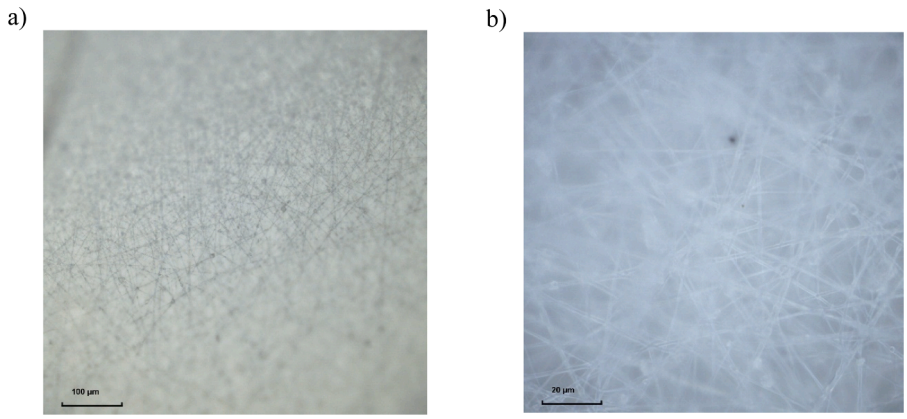

Fig. 11. Image of the G03 sample after firing in a furnace taken with a confocal microscope, magnification a) 20x, b) 100x.

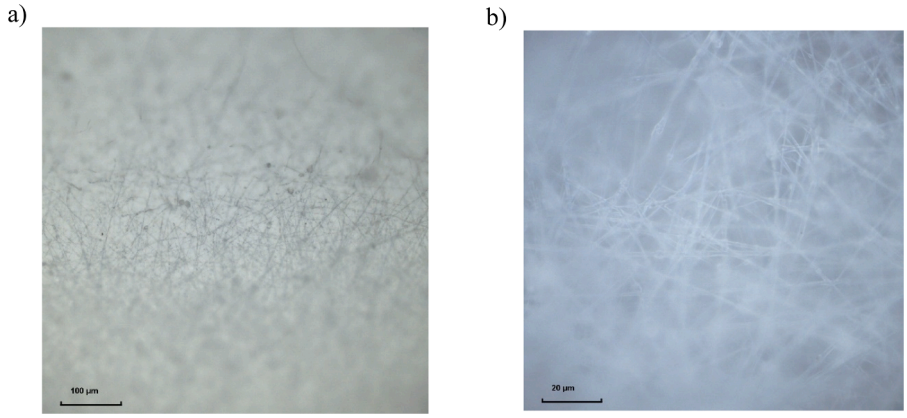

Fig. 12. Image of the G04 sample after firing in a furnace taken with a confocal microscope, magnification a) 20x, b) 100x.

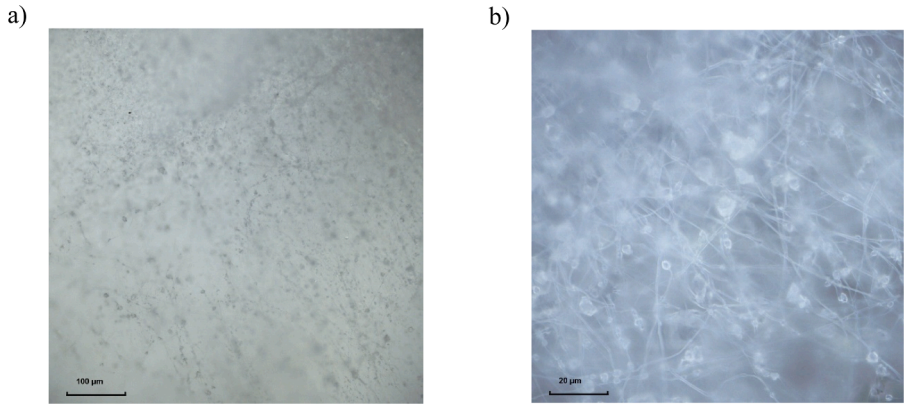

Fig. 13. Image of the G05 sample after firing in a furnace taken with a confocal microscope, magnification a) 20x, b) 100x.

morphologies. It is not possible to guarantee the homogeneity of all samples during fiber production, as factors such as laboratory temperature, relative humidity, and others play an important role. This inhomogeneity also explains the absence of the absorption edge in the measured samples, as photons from the radiation source can pass through the free space between fibers or be reflected from the fibers to the detector even at very low wavelengths.

4. Conclusion

This study aims were to prepare and analyze luminescent micro/nanofibrous layers via electrospinning. The process involved glass melting and grinding to obtain particles with the required size distribution, incorporating these particles into a polymer matrix, and producing micro/nanofibers using electrospinning. The layers were then examined using confocal laser microscopy and scanning electron microscopy to analyze their morphology and structure, followed by testing their optical and luminescent properties.

The results of this study provide valuable insights into the characteristics and potential applications of the developed micro/nanofiber layers. These layers, which incorporate luminescent micro and nanoparticles, have shown significant potential for absorbing and emitting

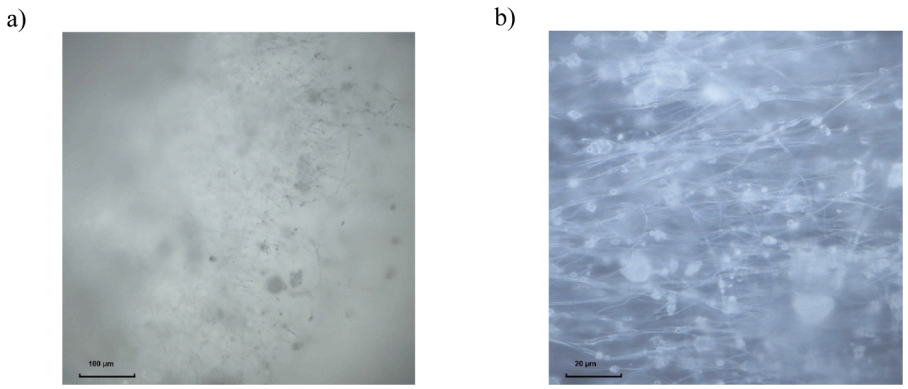

Fig. 14. Image of the G06 sample after firing in a furnace taken with a confocal microscope, magnification a) 20x, b) 100x.

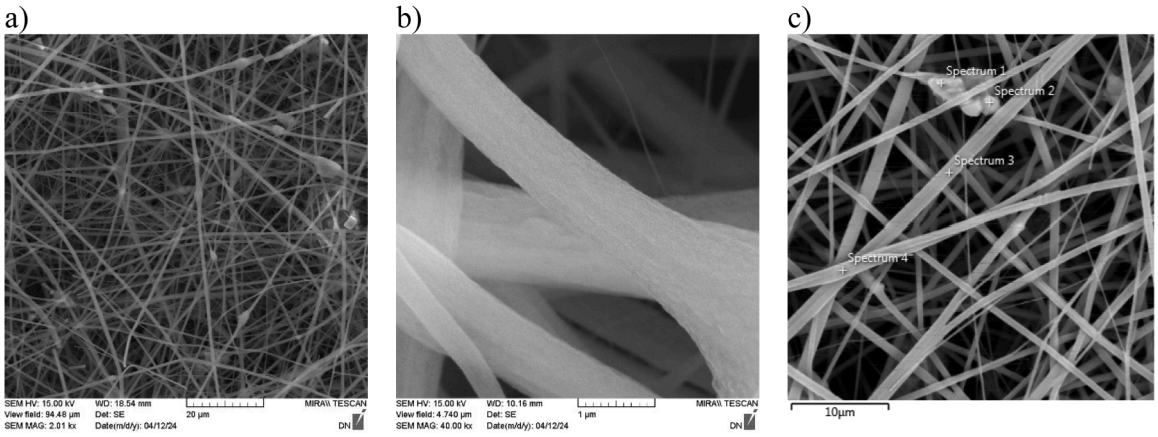

Fig. 15. Image from scanning electron microscopy of the G01 sample after firing in a furnace, a) 20x, b) 100x, c) Image from scanning electron microscopy of the G01 sample after firing in a furnace used for EDS analyses.

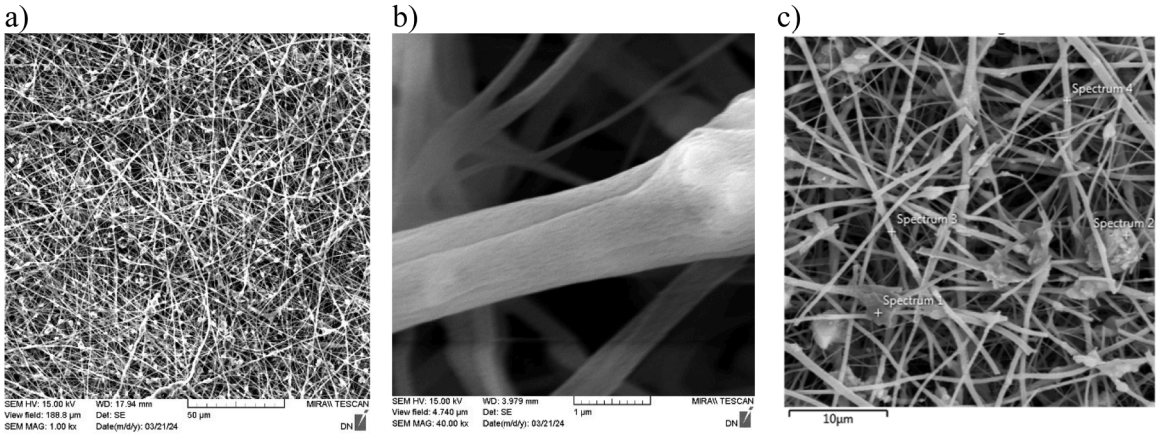

Fig. 16. Image from scanning electron microscopy of the G02 sample after firing in a furnace, a) 20x, b) 100x, c) Image from scanning electron microscopy of the G02 sample after firing in a furnace used for EDS analyses.

radiation, which is critical for their future use in both science and medicine. A comprehensive analysis of the fiber production process, including their morphology, structure, and chemical composition, uncovered specific properties that are vital for further development and practical application. The research detailed the grinding process of the glasses and the determination of particle size distribution necessary to achieve the desired morphology of the micro/nanofiber layers. Furthermore, the samples were analyzed using techniques such as laser confocal microscopy and scanning electron microscopy, which provided deeper insights into the morphology and structure of the fibers produced. The findings revealed that both the diameter of the fibers and the distribution of particles within them can vary based on production conditions, indicating opportunities for further optimization. Photodynamic therapy represents a promising area for the application of these materials, as prior studies have demonstrated the effectiveness of luminescent glasses. Future investigations should focus on more extensive testing of these fibers in combination with various photosensitive agents and their responses to light, aiming to better understand and

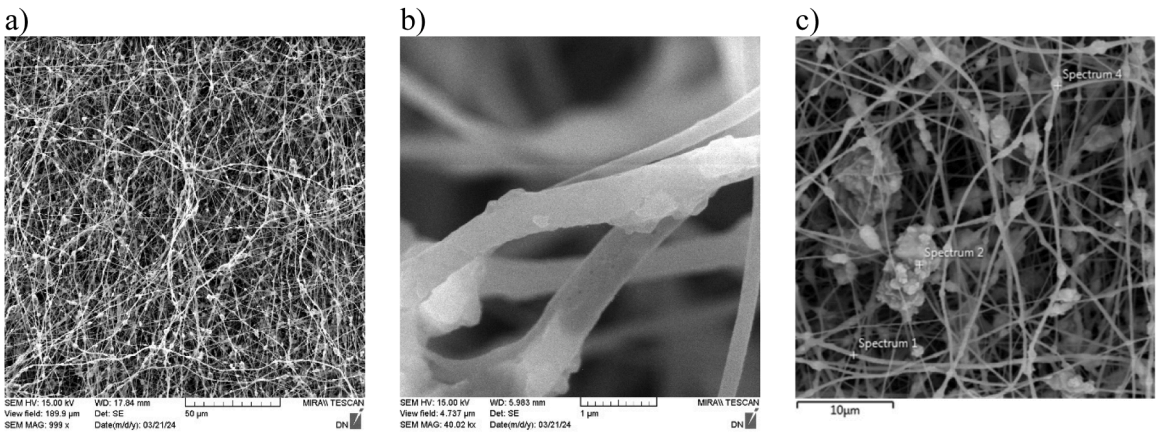

Fig. 17. Image from scanning electron microscopy of the G03 sample after firing in a furnace, a) 20x, b) 100x, c) Image from scanning electron microscopy of the G03 sample after firing in a furnace used for EDS analyses.

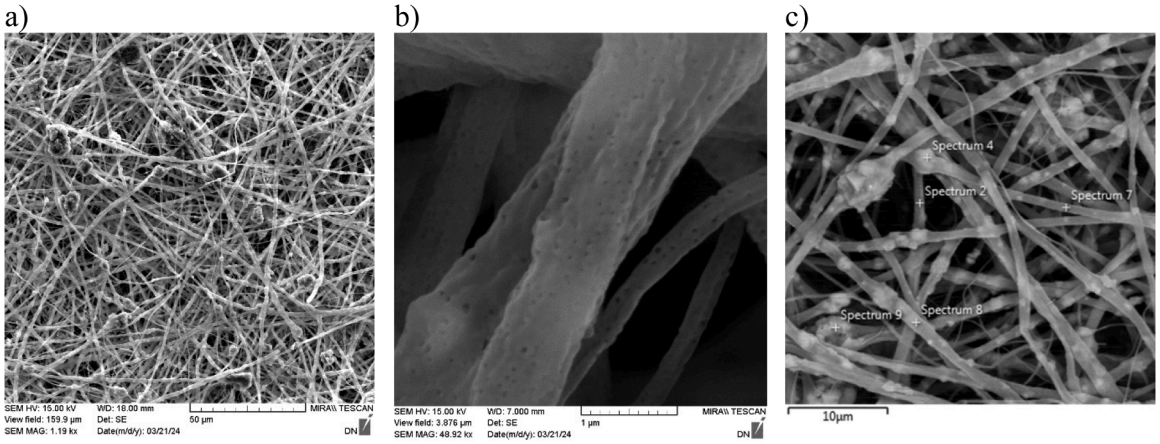

Fig. 18. Image from scanning electron microscopy of the G04 sample after firing in a furnace, a) 20x, b) 100x, c) Image from scanning electron microscopy of the G04 sample after firing in a furnace used for EDS analyses.

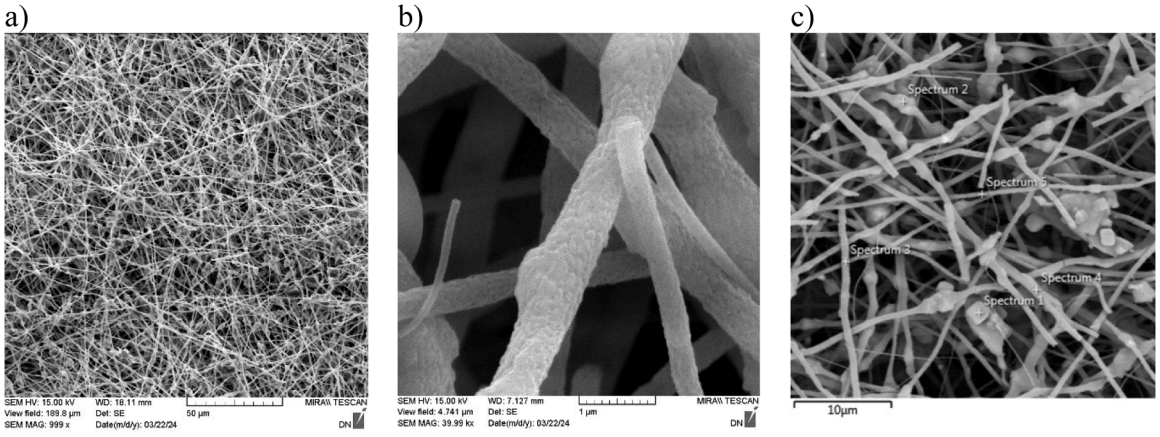

Fig. 19. Image from scanning electron microscopy of the G05 sample after firing in a furnace, a) 20x, b) 100x, c) Image from scanning electron microscopy of the G05 sample after firing in a furnace used for EDS analyses.

exploit their properties for innovative therapeutic methods. In a clinical context, incorporating these micro/nanofiber layers could significantly improve the efficacy and safety of photodynamic therapy. This research thus paves the way for new innovations in the treatment of cancer and other serious illnesses, offering renewed hope for patients around the globe.

CRediT authorship contribution statement

Aiman Albekova: Writing – original draft. **Martin Havlík Míka:** Writing – review & editing, Conceptualization. **Kristýna Jílková:** Writing – review & editing. **Richard Bursa:** Writing – review & editing. **Dominika Fink:** Writing – review & editing.

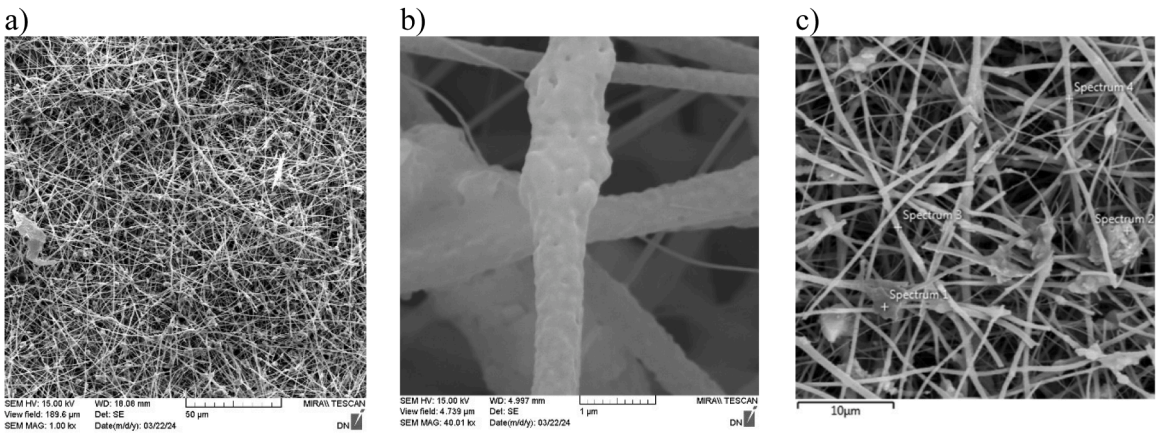

Fig. 20. Image from scanning electron microscopy of the G06 sample after firing in a furnace, a) 20x, b) 100x, c) Image from scanning electron microscopy of the G06 sample after firing in a furnace used for EDS analyses.

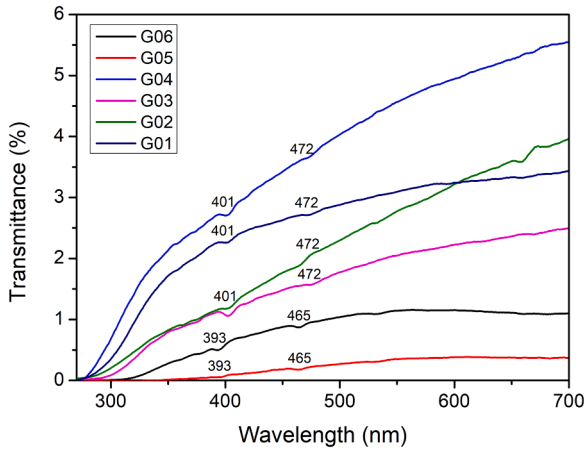

Fig. 21. Transmittance spectra of fibers G01-G06.

Declaration of competing interest

The authors declare that they have no known competing financial interests or personal relationships that could have appeared to influence the work reported in this paper.

Acknowledgments

This work was financially supported from the grants of Specific university research – grant N№ A2_FCHT_2024_079 and N№ A1_FCHT_2024_008.

References

[1] D. Begmatova, H. Eshkuvatov, N. Abdullayev, N. Xodjayeva, O. Suvonova, J. Ishtayev, Use of educational technologies in teaching the basics of nanophysics, nanomaterials and nanotechnologies, Results Opt. 16 (2024), https://doi.org/10.1016/j.rio.2024.100717 vol.

[2] S. Pang, L. Zhao, Y. An, Advanced developments in nanotechnology and nanomaterials for the oil and gas industry: a review, Geoenergy Sci. Eng. 238 (2024), https://doi.org/10.1016/j.geoen.2024.212872 vol.

[3] G. Niu, H. Wang, Y. Zhai, B. Zhou, Y. Kang, Pei Zh, X. Ji, Nanotechnology-based in situ cancer vaccines: mechanisms, design, and recent advances, Nanotoday 56 (2024), https://doi.org/10.1016/j.nantod.2024.102286 vol.

[4] A. Hajjafari, S. Sadr, A. Rahdar, M. Bayat, N. Lotfalizadeh, S. Dianaty, A. Rezaei, S. Partovi Moghaddam, K. Hajjafari, P. Ahmadi Simab, Z. Kharaba, H. Borji, S. Pandey, Exploring the integration of nanotechnology in the development and application of biosensors for enhanced detection and monitoring of colorectal cancer, Inorg. Chem. Commun. 164 (2024), https://doi.org/10.1016/j.inoche.2024.112409 vol.

[5] Y. Huang, W. Ouyang, Z. Lai, G. Qiu, Zh Bu, X. Zhu, O. Wang, Y. Yu, J. Liu, Nanotechnology-enabled sonodynamic therapy against malignant tumors, Nanoscale Adv 6 (8) (2024) 1974–1991, https://doi.org/10.1039/d3na00738c, volIssue16 AprilPages.

[6] J. Zhao, J. Shi, X. Meng, C. Gong, P. Wu, Z. Yang, H. Dong, ROS-activated nanoscale coordination polymers for enhanced ultrasound-mediated therapy for the treatment of cancer, Acta Biomater 143 (2022) 372–380, https://doi.org/10.1016/j.actbio.2022.02.030, vol15 AprilPages.

[7] M. Xianbin, T. Zhang, W. Qiu, M. Liang, Y. Gao, P. Xue, Y. Kang, Zh. Xu, Bioresponsive prodrug nanogel-based polycondensate strategy deepens tumor penetration and potentiates oxidative stress, J. Chem. Eng. 420 (2021), https://doi.org/10.1016/j.cej.2020.127657 volPart 2.

[8] L. Rengeng, Z. Qianyu, L. Yuehong, P. Zhongzhong, L. Libo, Sonodynamic therapy, a treatment developing from photodynamic therapy, Photodiagn. Photodyn. 19 (2017) 159–166, https://doi.org/10.1016/j.pdpdt.2017.06.003. Pages.

[9] V. Tayebi-Khorrami, P. Rahmanian-Devin, M. Reza Fadaei, J. Movaffagh, V. Reza Askari, Advanced applications of smart electrospun nanofibers in cancer therapy: with insight into material capabilities and electrospinning parameters, Int. J. Pharm-X. 8 (2024), https://doi.org/10.1016/j.ijpx.2024.100265 vol.

[10] L. Jianxin, C. Xuedi, Zh Xiaolei, J. Xicheng, J. Hengzhe, F. Junlin, Review on functional electrospun nanofibers: theory, application and fabrication, Mater. Sci. Eng. B. 307 (2024), https://doi.org/10.1016/j.mseb.2024.117488 vol.

[11] J. Kang, N. Deng, B. Cheng, W. Kang, Progress in the application of polymer fibers in solid electrolytes for lithium metal batteries, J. Energy Chem. 92 (2024) 26–42, https://doi.org/10.1016/j.jechem.2023.12.035, volPages.

[12] Z. Cai, Y. Bai, A.D. Almutairi, C. Ding, Low-high-low cyclic performance of screw connections for fibre-polymer composites, Constr. Build. Mater. 419 (2024), https://doi.org/10.1016/j.conbuildmat.2024.135454 vol.

[13] M.R. Sanjay, S. Siengchin, J. Parameswaranpillai, M. Jawaid, C. Iulian Pruncu, A. Khan, A comprehensive review of techniques for natural fibers as reinforcement in composites: preparation, processing and characterization, Carbohydr. Polym. 207 (2019) 108–121, https://doi.org/10.1016/j.carbpol.2018.11.083, volPages.

[14] Q. Zhang, B. Shi, J. Ding, L.P. Yan, Y. Thawani, C. Fu, X. Chen, Polymer scaffolds facilitate spinal cord injury repair, Acta Biomater 88 (2019) 57–77, https://doi.org/10.1016/j.actbio.2019.01.056, volPages.

[15] O.S. Ahmad, T.S. Bedwell, C. Esen, A. Garcia-Cruz, S.A. Piletsky, Molecularly imprinted polymers in electrochemical and optical sensors, Trends Technol. 37 (3) (2019) 294–309, https://doi.org/10.1016/j.tibtech.2018.08.009, volIssuePages.

[16] H. Pan, X. Wang, S. Jia, Z. Lu, J. Bian, H. Yang, L. Han, H. Zhang, Fiber-induced crystallization in polymer composites: a comparative study on poly(lactic acid) composites filled with basalt fiber and fiber powder, Int. J. Biol. Macromol. 183 (2021) 45–54, https://doi.org/10.1016/j.ijbiomac.2021.04.104, volPages.

[17] M. Babazadeh-Mamaqani, D. Razzaghi, H. Roghani-Mamaqani, A. Babaie, M. Rezaei, R. Hoogenboom, M. Salami-Kalajahi, Photo-responsive electrospun polymer nanofibers: mechanisms, properties, and applications, Prog. Mater. Sci. 146 (2024), https://doi.org/10.1016/j.pmatsci.2024.101312.

[18] T. Wu, M. Ding, C. Shi, Y. Qiao, P. Wang, R. Qiao, X. Wang, J. Zhong, Resorbable polymer electrospun nanofibers: history, shapes and application for tissue engineering, Chin. Chem. Lett. 31 (3) (2020) 617–625, https://doi.org/10.1016/j.cclet.2019.07.033, volIssuePages.

[19] F.A. Janjhi, I. Chandio, D. Janwery, V. Vatanpour, R. Castro-Muñoz, A review on hydrophobic electrospun nanofibers-based materials and membranes for water treatment: challenges, outlook, and stability, Sep, Purif. Technol. 353 (2025), https://doi.org/10.1016/j.seppur.2024.128370 volPart A.

[20] N.N. Safi, B.I. Waisi, Preparation of electrospun double-layer PVDF:PMMA membrane non-woven nanofibers for desalination by membrane distillation process, Desal. Water Treat. 314 (2023) 49–58, https://doi.org/10.5004/dwt.2023.30063, volPages.

[21] W. Du, T. Wang, S. Hu, J. Luan, F. Tian, G. Ma, J. Xue, Engineering of electrospun nanofiber scaffolds for repairing brain injury, Eng. Regen. 4 (3) (2023) 289–303, https://doi.org/10.1016/j.engreg.2023.04.001, volIssuePages.

[22] R. Castro-Muñoz, M.S. Kharazmi, S.M. Jafari, Chitosan-based electrospun nanofibers for encapsulating food bioactive ingredients: a review, Int. J. Biol. Macromol. 245 (2023), https://doi.org/10.1016/j.ijbiomac.2023.125424 vol.
[23] N. Aminu, S. Ilyasu, M. Al-Kassim Hassan, F.S. Kurfi, A.I. Jatau, S. Chan, D. Alfred-Ugbenbo, Applications of nanofibers drug delivery system in cancer therapy, J. Drug Deliv. Technol. 90 (2023), https://doi.org/10.1016/j.jddst.2023.105128 volDecember.
[24] V. Rahimkhoei, M. Padervand, M. Hedayat, F. Seidi, E.A. Dawi, A. Akbari, Biomedical applications of electrospun polycaprolactone-based carbohydrate polymers: a review, Int. J. Biol. Macromol. 253 (2023), https://doi.org/10.1016/j.ijbiomac.2023.126642 volPart 1.
[25] D. Švára, B. Filipová, P. Jelínek, P. Mikeš, A. Kluk, M. Šoóš, The impact of polymer mixture composition on the properties of electrospun membranes for drug delivery applications, Int. J. Pharm. 647 (2023), https://doi.org/10.1016/j.ijpharm.2023.123548 vol.
[26] G. Liu, Z. Gu, Y. Hong, L. Cheng, C. Li, Electrospun starch nanofibers: recent advances, challenges, and strategies for potential pharmaceutical applications, J. Control. Release 252 (2017) 95–107, https://doi.org/10.1016/j.jconrel.2017.03.016, volPages.
[27] C. Ao, Y. Niu, X. Zhang, X. He, W. Zhang, C. Lu, Fabrication and characterization of electrospun cellulose/nano-hydroxyapatite nanofibers for bone tissue engineering, Int. J. Biol. Macromol. 97 (2017) 568–573, https://doi.org/10.1016/j.ijbiomac.2016.12.091, volPages.
[28] J. Lin, L. Yang, X. Hu, H. Peng, H. Ren, T. Li, C. Lou, Photodynamic antibacterial micro/nanofiber composite membrane with high efficiency and low resistance filtration performance for medical protective materials, J. Ind. Eng. Chem 128 (2023) 184–195, https://doi.org/10.1016/j.jiec.2023.07.047, volPages.
[29] Y. Guo, J. Zheng, Zh Wang, G. Chen, K. Hou, M. Zhu, Biocompatible optical fiber for photomedical application, Giant 16 (2023) 100195, https://doi.org/10.1016/j.giant.2023.100195 vol.
[30] Agrahari V., Agrahari V., Meng J., Mitra A.K., Chapter 9 - electrospun nanofibers in drug delivery: fabrication, advances, and biomedical applications, emerging nanotechnologies for diagnostics, drug delivery and medical devices, Micro Nano Technol., 2017, Pages 189–215. https://doi.org/10.1016/B978-0-323-42978-8.00009-7.
[31] M. Maleki, A. Natalello, R. Pugliese, F. Gelain, Fabrication of nanofibrous electrospun scaffolds from a heterogeneous library of co-and self-assembling peptides, Acta Biomater 51 (2017) 268–278, https://doi.org/10.1016/j.actbio.2017.01.038, volPages.
[32] M.P. Ribeiro, D.R. Figueira, S.S. Silva, R.F. Pereira, T. Silva, H. Reis, L. R, Electrospun nanofibers impregnated with silver nanoparticles as dressings for infected chronic wounds, Mater. Sci. Eng. C 32 (4) (2012) 929–935, https://doi.org/10.1016/j.msec.2012.01.006. Pages.
[33] W. Fan, Y. Li, H. Li, Z. Cheng, Y. Zhang, H. Ma, J. Lin, Sm-doped germanate glass channel waveguide as light source for minimally invasive photodynamic therapy surgery, J. Lumin. 131 (5) (2011) 884–888, https://doi.org/10.1016/j.jlumin.2010.12.025. Pages.
[34] R. Singhal, R. Kumar, S.K. Dhawan, Luminescence and dielectric behavior of Sm_2O_3 nanocrystals synthesized by the citrate-nitrate auto-combustion method, J. Alloys Compd. 492 (1–2) (2010), https://doi.org/10.1016/j.jallcom.2009.11.084. L6–L10.
[35] X. Liu, T. Lin, Y. Gao, Z. Xu, G. Yao, Development of rare-earth doped glass nanofibers for biophotonic applications, Nano-Struct. Nano-Obj. 34 (2023) 100971, https://doi.org/10.1016/j.nanoso.2023.100971.
[36] R. Mohammadi, M. Rezaei, M. Bagheri, Electrospun luminescent nanofibers for biomedical applications, J. Appl. Polym. Sci. 136 (23) (2019) 47691, https://doi.org/10.1002/app.47691.
[37] A. Kamkaew, S.H. Lim, H.B. Lee, L.V. Kiew, L.Y. Chung, K. Burgess, Photodynamic therapy in cancer: emerging trends in development of smart light delivery systems, Chem. Soc. Rev. 42 (1) (2013) 77–88, https://doi.org/10.1039/C2CS35242H. Pages.
[38] Albekova A., Optimization of luminescence of phosphor glasses for photodynamic therapy, Diploma thesis, 2020.
[39] Klusoňová N., Luminescence of lanthanides in silicate glass containing Zn, Ge, and Bi, Diploma thesis, 2021.
[40] A. Albekova, K. Jilkova, M. Havlik Mika, Luminescent phosphor glasses with Sm2O3 for photodynamic therapy application, Ceram. Int. 51 (2025) 506–511, https://doi.org/10.1016/j.ceramint.2024.11.028, vol.